

Geophysical Research Letters

RESEARCH LETTER

10.1002/2017GL076008

Key Points:

- The superposition of M_2 and S_2 internal tides forms a spring-neap cycle, whose frequency, wave number, and phase are the M_2 and S_2 differences
- The spring-neap cycle and energy of the semidiurnal internal tide propagate at the group velocity
- · Phase and group velocities determined from satellite altimetry agree with theoretical values estimated using the WOA13 ocean stratification

Supporting Information:

- · Supporting Information S1
- Movie S1
- Data Set S1

Correspondence to:

zzhao@apl.washington.edu

Citation:

Zhao Z. (2017). Propagation of the semidiurnal internal tide: Phase velocity versus group velocity. Geophysical Research Letters, 44, 11,942-11,950. https://doi.org/10.1002/2017GL076008

Received 10 OCT 2017 Accepted 16 NOV 2017 Accepted article online 22 NOV 2017 Published online 14 DEC 2017

Propagation of the Semidiurnal Internal Tide: Phase Velocity Versus Group Velocity

Zhongxiang Zhao¹



¹Applied Physics Laboratory, University of Washington, Seattle, WA, USA

Abstract The superposition of two waves of slightly different wavelengths has long been used to illustrate the distinction between phase velocity and group velocity. The first-mode M_2 and S_2 internal tides exemplify such a two-wave model in the natural ocean. The M_2 and S_2 tidal frequencies are 1.932 and 2 cycles per day, respectively, and their superposition forms a spring-neap cycle in the semidiurnal band. The spring-neap cycle acts like a wave, with its frequency, wave number, and phase being the differences of the M_2 and S_2 internal tides. The spring-neap cycle and energy of the semidiurnal internal tide propagate at the group velocity. Long-range propagation of M_2 and S_2 internal tides in the North Pacific is observed by satellite altimetry. Along a 3,400 km beam spanning $24^{\circ} - 54^{\circ}$ N, the M_2 and S_2 travel times are 10.9 and 11.2 days, respectively. For comparison, it takes the spring-neap cycle 21.1 days to travel over this distance. Spatial maps of the M_2 phase velocity, the S_2 phase velocity, and the group velocity are determined from phase gradients of the corresponding satellite observed internal tide fields. The observed phase and group velocities agree with theoretical values estimated using the World Ocean Atlas 2013 annual-mean ocean stratification.

1. Introduction

Observations of group velocity and phase velocity of water surface waves were first reported by S. J. Russesll (see page 369 in Russell, 1844). The distinction was elegantly explained by Stokes (1876) and Rayleigh (1877) using the superposition of two waves of slightly different wavelengths (hereinafter "two-wave model"). In this model, the two-wave superposition forms a slowly varying envelope: Group velocity is the propagation speed of the envelope and phase velocity is the propagation speed of individual waves (see Figure 62 in Lighthill, 1978). In a more general sense, phase velocity C_p and group velocity C_q can be derived from any given dispersion relation $\omega(k)$ following

$$C_{p} \equiv \frac{\omega}{k} \tag{1}$$

and

$$C_g \equiv \frac{d\omega}{dk},\tag{2}$$

where k and ω are wave number and frequency, respectively. The physical meaning of group velocity was first reported by Reynolds (1877), who demonstrated that group velocity is the speed at which the wave energy is transported. Since then, these concepts have been applied to a variety of wave motions such as sound waves and electromagnetic waves. Due to its simplicity and clarity, the two-wave model has been employed widely to illustrate the distinction of phase velocity and group velocity (Gill, 1982; Lamb, 1916; Lighthill, 1978). Although observations of surface dispersive waves have long been reported (Russell, 1844), there is no report of the two-wave superposition in the real ocean, most likely because surface waves are broadband, consisting of multiple monochromatic waves.

This paper reports on a pair of waves, whose superposition gives evidence for the existence of such a two-wave model in the natural ocean. They are the first-mode M_2 and S_2 internal tides. Internal tides are generated when barotropic tidal currents flow over rough bottom topography (Garrett & Kunze, 2007). The first-mode internal tides contain most of the converted tidal energy and may propagate O(1,000) km away from their generation sites. Internal tides have the same frequencies as their surface counterparts. M2 and S2 are the two largest

©2017. American Geophysical Union. All Rights Reserved.

Table 1 Long-Range Propagation of the Semidiurnal Internal Tide Over a 3,400 km Distance Spanning 24° – 54° N

	Period	Frequency	Travel time	Mean velocity	Mean Wavelength	
Wave	(hour)	(cycle/day)	(day)	(m/s)	(km)	Remark
M ₂	12.421	1.932	10.9 (11.1)	3.62 (3.55)	162 (159)	Phase velocity
S_2	12	2	11.2 (11.4)	3.51 (3.45)	152 (149)	Phase velocity
SN	354.367	0.068	21.1 (20.4)	1.87 (1.93)	2,380 (2,460)	Group velocity

Note. The observed values are from the along-beam travel times determined in Figure 3d. The theoretical values (given in parentheses) are calculated from along-beam theoretical velocities shown in Figure 1. SN stands for the spring-neap cycle.

constituents in the semidiurnal band. Their frequencies are 1.932 and 2 cycles per day (cpd), respectively, with a difference of 0.068 cpd (Table 1). It is well known that the surface semidiurnal tide has a spring-neap cycle of about 14.7 days. In this paper, it will be demonstrated that the superposition of M_2 and S_2 internal tides also exhibits a spring-neap cycle in the semidiurnal band. Observations of M_2 and S_2 internal tides and the spring-neap cycle are from satellite altimetry (Zhao et al., 2016; Zhao, 2017), which detects coherent internal tides via their sea surface height (SSH) fluctuations (Ray & Mitchum, 1996).

The novelty of this paper lies in the following two aspects:

- 1. This paper reports a real case of the two-wave model in the natural ocean and develops the model by examining its phase information. The classic two-wave model usually omits the phase information of the waves (Rayleigh, 1877; Stokes, 1876). In this paper, it is demonstrated that the spring-neap cycle acts like a wave, whose frequency, wave number, and phase are the differences of M_2 and S_2 . This new finding allows us to track the long-range propagation of the spring-neap cycle, as well as the M_2 and S_2 internal tides.
- 2. This paper highlights a new technique for observing the phase and group velocities of internal tides. The internal tide's propagation velocities have been calculated theoretically using the Sturm-Liouville equation and ocean stratification (e.g., Chelton et al., 1998; Rainville & Pinkel, 2006). This paper shows that the phase and group velocities of internal tides can be calculated directly from phase gradients of the internal tide fields observed by satellite altimetry. The results show that in the North Pacific, the observed and theoretical velocities agree very well.

This paper is organized as follows. Section 2 simply describes the theoretical phase and group velocities. Section 3 presents the satellite observed M_2 and S_2 internal tides, their long-range propagation, and the spring-neap cycle. Section 4 gives a new technique for calculating the phase and group velocities from satellite observed internal tide fields. Section 5 contains a summary, and section 6 discusses implications of this work.

2. Theoretical Velocities

The dynamics theory of internal tides has long been well established (Gill, 1982; Munk, 1981; Olbers, 1983; Wunsch, 1975). A linear internal tide can be decomposed into a series of orthogonal baroclinic modes, each of which has a vertical modal structure and propagates in the horizontal direction like a wave in a homogeneous fluid. Assuming a flat bottom H and a stratification profile N(z), the orthogonal vertical mode $\Phi(z)$, and eigenvalue velocity C can be obtained by solving the Sturm-Liouville equation

$$\frac{d^2\Phi(z)}{dz^2} + \frac{N^2(z)}{C^2}\Phi(z) = 0$$
 (3)

subject to the rigid-lid boundary condition $\Phi(0) = \Phi(-H) = 0$ (Gill, 1982). In this paper, the ocean stratification profile N(z) is from the annual-mean hydrography in the World Ocean Atlas 2013 (WOA13) (Locarnini et al., 2013; Zweng et al., 2013). The ocean depth H is from the 2 arc min topography database compiled from shipboard survey and satellite altimetry (Smith & Sandwell, 1997). Equation (3) yields a series of discrete vertical modes $\Phi_n(z)$ and eigenvalue velocities C_n , where the subscript n denotes the mode number. This paper focuses on the first-mode M_2 and S_2 internal tides (n = 1, omitted herein).

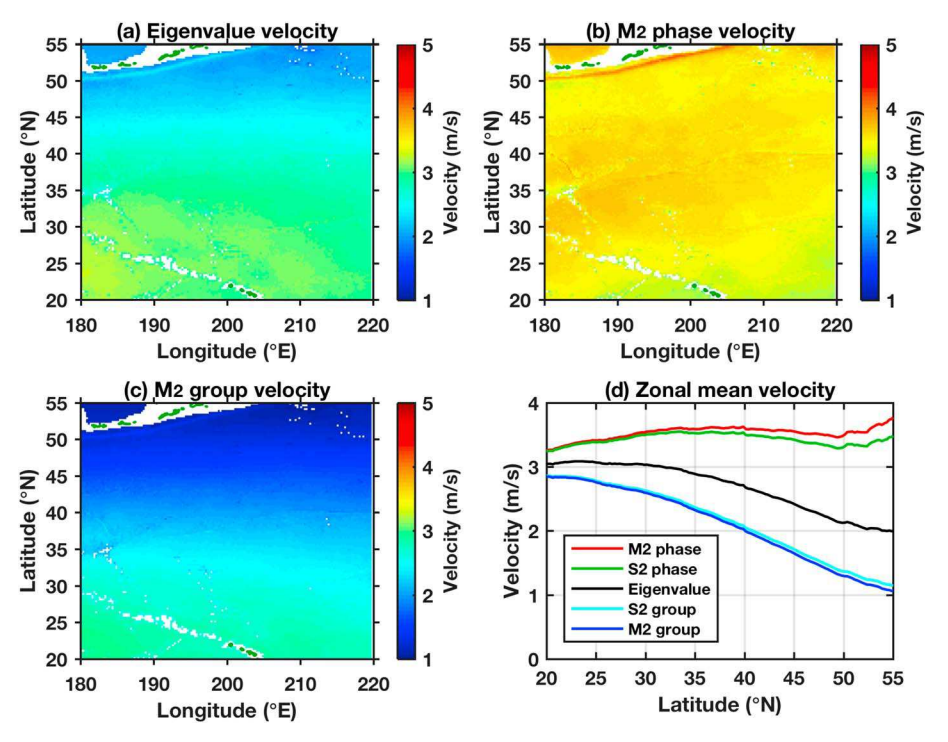


Figure 1. Theoretical velocities estimated using the Sturm-Liouville equation and the WOA13 annual-mean stratification. (a) Eigenvalue velocity. (b) Phase velocity and (c) group velocity of the M_2 internal tide. The S_2 phase velocity and group velocity are not shown, but their zonal means are given. (d) Zonal-mean velocities in the North Pacific Ocean (180° – 220°E). In all panels, velocities in waters shallower than 3,000 m are discarded.

Without the Earth's rotation, the long-range propagating internal tide is nondispersive, with its phase velocity and group velocity equal to eigenvalue speed C. With the Earth's rotation, the internal tide in the horizontal direction has a dispersion relation as Poincaré waves (Gill, 1982)

$$\omega^2 = f^2 + C^2 k^2,\tag{4}$$

where ω and f are the tidal and inertial frequencies, respectively. Note that $f \equiv 2\Omega \sin(\text{latitude})$, where Ω is the Earth's rotation rate. By the definition given in equations (1) and (2), phase and group velocities can be calculated following

$$C_p \equiv \frac{\omega}{k} = \frac{\omega}{\sqrt{\omega^2 - f^2}} C(N, H)$$
 (5)

and

$$C_g \equiv \frac{d\omega}{dk} = \frac{\sqrt{\omega^2 - f^2}}{\omega} C(N, H). \tag{6}$$

These equations reveal that both phase velocity and group velocity are functions of ω and f, as well as N(z)and H. It is apparent that group velocity is always less than eigenvalue velocity and that phase velocity is always greater than eigenvalue velocity.

The eigenvalue velocity of the first-mode internal tide in the North Pacific varies little in the zonal direction, but greatly in the meridional direction (Figure 1a). This is because the ocean stratification weakens with increasing latitude. Note that the ocean stratification is only used in equation (3) to determine the vertical structures and eigenvalue velocities. The phase and group velocities of the M_2 internal tide, calculated using equations (5) and (6), are shown in Figures 1b and 1c, respectively. Those of the S2 internal tide have similar spatial patterns but different amplitudes (not shown). Figure 1d shows the zonal-mean velocities over 180° - 220° E: the eigenvalue velocity, the M_2 and S_2 phase velocities, and the M_2 and S_2 group velocities. While the eigenvalue velocity and the group velocities decrease monotonically with latitude, the phase velocities exhibit a

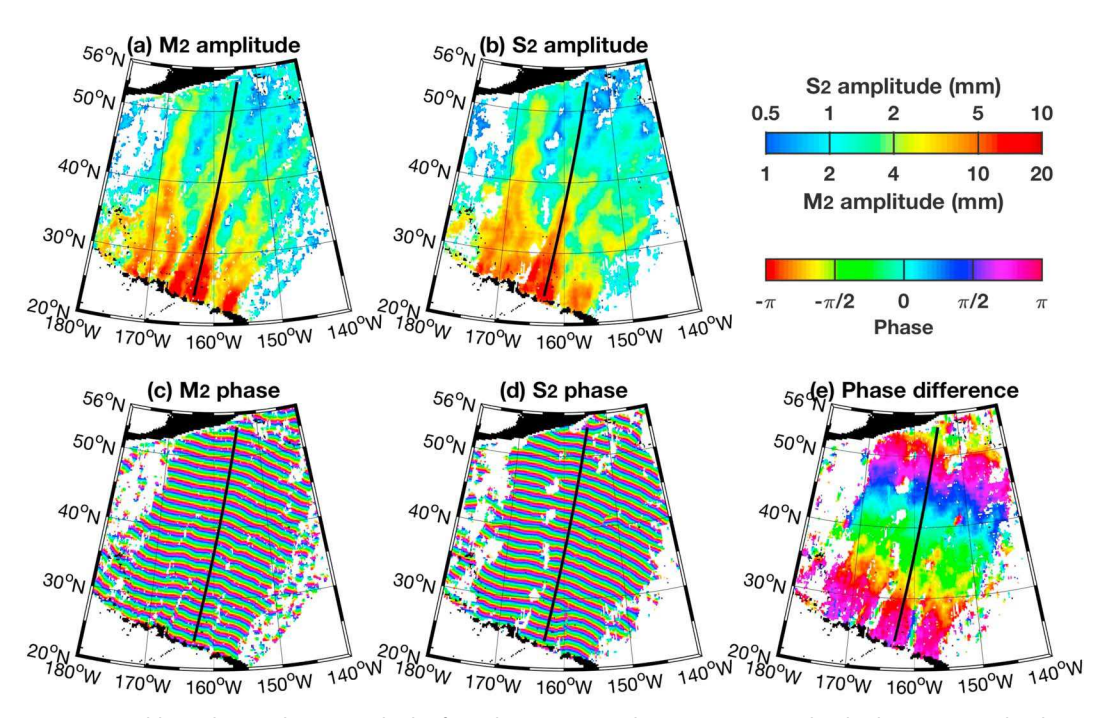


Figure 2. Northbound M_2 and S_2 internal tides from the Hawaiian Ridge. (a) M_2 SSH amplitude. (b) S_2 SSH amplitude. M_2 and S_2 are plotted using the same colormap, but the M_2 range is twice that of the S_2 . Internal tides of small amplitude $(M_2 < 1 \text{ mm}; S_2 < 0.5 \text{ mm})$ are discarded. (c) M_2 phase. (d) S_2 phase. (e) The phase difference between S_2 and M_2 .

latitudinal fluctuation. They increase in 20° – 35°N, decrease in 35° – 50°N, and again increase beyond 50°N. This fluctuation is due to the counteraction of ocean stratification N(z) and the Earth's rotation f: the former causes a decreasing trend, while the latter causes an increasing trend. Another remarkable feature is that the differences of the M_2 and S_2 velocities (both phase and group velocities) increase with latitude.

3. Satellite Observations

3.1. M_2 and S_2 Internal Tides

Internal tides have O(10 m) isopycnal displacements in the ocean interior. In contrast, their SSH fluctuations are only about a few centimeters. This centimeter-scale SSH signal can be detected by satellite altimetry (Ray & Mitchum, 1996). Satellite altimetry thus yields regional two-dimensional internal tide fields. During 1992 – 2012, there are about 50 satellite years of SSH measurements collected by multiple satellite missions. By a plane wave fit method (Ray & Cartwright, 2001; Zhao et al., 2016), the global mode-1 M_2 and S_2 internal tides have been constructed in previous studies (Zhao et al., 2016; Zhao, 2017).

The plane wave fit method extracts multiple waves of different propagation directions in one given fitting window. It thus resolves multiwave interference (Zhao et al., 2016). Figure 2 shows the northbound M_2 and S_2 internal tides in the North Pacific Ocean (propagation direction ranging 40° – 100° north of east). The southbound internal tides are extracted as well but excluded in this paper. Figure 2 shows that the M_2 and S_2 internal tides originate at the 2,500 km long Hawaiian Ridge. Both can travel over 3,500 km from the Hawaiian Ridge. Their amplitudes are not uniform in space. There are some remarkable internal tidal "beams," which are from strong generation sites at the Hawaiian Ridge (Merrifield & Holloway, 2002; Zhao, 2017). In this region, the M_2 amplitudes are about twice the S_2 amplitudes (Zhao, 2017). Figures 2c and 2d show periodic isophase lines extending from Hawaii to Alaska, consistent with their transbasin propagation.

3.2. Spring-Neap Cycle

The superposition of M_2 and S_2 internal tides forms a spring-neap cycle along one section (Figure 2, magenta line). This section was chosen because it follows a beam from Nihoa Island, Hawaii (Merrifield & Holloway, 2002; Zhao, 2017). The M_2 and S_2 phases increase northward, consistent with their northbound propagation (Figure 3a). Both of the M_2 and S_2 amplitudes decrease with propagation distance. Figure 3b shows their superposition using the observed decreasing amplitudes. Here the spring-neap cycle is not apparent, because both

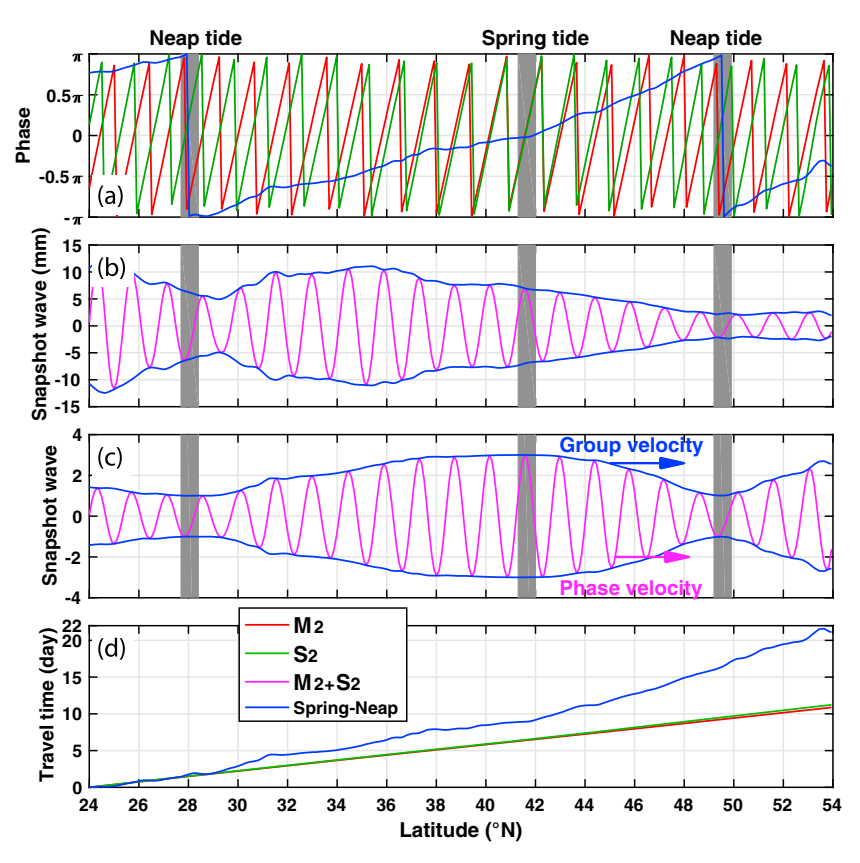


Figure 3. The superposition of M_2 and S_2 internal tides along one beam from the Hawaiian Ridge. See Figure 2 for the beam location. (a) Phase of M_2 , S_2 , and the spring-neap cycle. (b) Snapshot waveform of the superposed M_2 and S_2 internal tides. Blue lines indicate the envelope. (c) As in Figure 3b but that using the spatially invariant amplitudes (with an M_2 to S_2 ratio of 2:1) to highlight the spring and neap tides. Phase velocity and group velocity are labeled. (d) Along-beam travel times as a function of latitude. A movie is given in supporting information (Movie S1) to show the northbound motion of the spring-neap cycle.

 M_2 and S_2 decay exponentially. Figure 3c shows their superposition but using spatially invariant amplitudes (M_2 : 2 mm; S_2 : 1 mm). It shows that the superposition forms an envelope (blue lines), like the two-wave model demonstrated by Stokes (1876) and Rayleigh (1877). Group velocity and phase velocity are labeled according to their definitions: The former is the speed of individual waves (magenta arrow); the latter is the speed of the envelope (blue arrow).

The classic two-wave model usually omits the phase information (e.g., equation (5.4.1) in Gill, 1982). Here I add phase (ϕ_m and ϕ_s) to the M_2 and S_2 internal tides. Their superposition follows

$$M_2 + S_2 = A_m e^{i(k_m x - \omega_m t - \phi_m)} + A_s e^{i(k_s x - \omega_s t - \phi_s)}$$

$$\tag{7}$$

$$= \left(A_m e^{i\left(\frac{\Delta k}{2}x - \frac{\Delta \omega}{2}t - \frac{\Delta \phi}{2}\right)} + A_s e^{-i\left(\frac{\Delta k}{2}x - \frac{\Delta \omega}{2}t - \frac{\Delta \phi}{2}\right)} \right) e^{i\left(\bar{k}x - \bar{\omega}t - \bar{\phi}\right)}, \tag{8}$$

where Δk , $\Delta \omega$, and $\Delta \phi$ are the differences between S_2 and M_2 , and \bar{k} , $\bar{\omega}$ and $\bar{\phi}$ are their respective means. The first part of equation (8) is the envelope (Figure 2b, blue lines), and the second part is the mean (magenta line). Note that the spring-neap cycle and the envelope have different oscillation periods. In fact, each envelope covers two spring-neap cycles (refer to Figure 3b) so that their parameters differ by a factor of 2. The spring-neap (SN) cycle can be written as

$$\mathsf{SN} = e^{\pm i(\Delta kx - \Delta \omega t - \Delta \phi)}. \tag{9}$$

The frequency of the spring-neap cycle is 0.068 cpd (i.e., a 14.7 day period). The phase of the spring-neap cycle (i.e., $\Delta \phi$) is shown as the blue line in Figure 3a. At the moment shown in Figure 3b, a spring internal



tide occurs around 42°N, where M_2 and S_2 are in phase (the phase difference is zero). Two neap internal tides appear around 28°N and 50°N, respectively, where M_2 and S_2 are out of phase (the phase difference is 180°).

The spring-neap cycle acts like a wave, which propagates northbound in the same manner as M_2 and S_2 internal tides. For example, its phase increases with latitude (Figure 2a, blue line), similar to the phases of M_2 (red) and S_2 (green). M_2 and S_2 travel at slightly different phase velocities as two monochromatic waves, while the spring-neap cycle (the envelope or energy) travels at the group velocity. This scenario can be observed in the two-dimensional phase map as well (Figure 2e). The phase map of the spring-neap cycle in the North Pacific is similar to the phase maps of M_2 and S_2 , except that the spring-neap cycle has a much longer wavelength.

3.3. Long-Range Propagation

The travel times of M_2 and S_2 internal tides are calculated following

$$\Delta t = \frac{T}{2\pi} \left[\hat{\phi} \left(\mathsf{lat}_2 \right) - \hat{\phi} \left(\mathsf{lat}_1 \right) \right], \tag{10}$$

where T is the tidal period and $\hat{\phi}$ the unwrapped phase (increase monotonically). This calculation is along the beam spanning 24° – 54°N (Figure 2). The resultant travel times are plotted with respect to latitude (Figure 3d). The M_2 and S_2 travel times are 10.9 and 11.2 days, respectively, with M_2 being about 0.3 day (\approx 7 h) faster. Because the spring-neap cycle has a period of 354.367 h, its travel time over this distance is about 21.1 days (Table 1). In other words, the energy of internal tides is transported across the North Pacific in about 21.1 days.

The along-beam distance between 24° and 54°N is about 3,400 km. From this distance and travel times, their mean speeds and mean wavelengths are calculated (Table 1). The mean velocities of M_2 , S_2 , and the spring-neap cycle are 3.62, 3.52, and 1.87 m/s, respectively. Their mean wavelengths are 162, 152, and 2,380 km, respectively. For comparison, the theoretical phase and group velocities along this beam are interpolated from Figure 1. Accordingly, the theoretical mean velocities, mean wavelengths, and travel times are calculated. In Table 1, the theoretical values are given in parentheses. The results show that the observed and theoretical values agree very well. Note that the wavelength of the slowly varying spring-neap cycle is much longer than the M_2 and S_2 wavelengths, because of its 354.367 h period. This example clarifies the phase and group velocities of the long-range propagating internal tides.

4. Phase Velocity and Group Velocity

Both phase velocity and group velocity are functions of latitude (Figure 1d). To investigate their latitudinal dependence, the phase and group velocities are determined using the phase maps shown in Figures 2c-2e. The calculation is conducted at regular grid of 0.5° longitude by 0.5° latitude. At each grid point, the M_2 and S_2 phase velocities are calculated from phase gradients. In practice, the propagation velocity and direction are determined by fitting plane waves. In each fitting window of 4° by 4° , plane waves are fitted to the phase map using directions ranging [40° , 110°] and the propagation direction is determine in terms of overall least squares. Similarly, plane waves are fitted using wavelengths ranging [100, 250] km to determine the propagation velocity. Thus, the direction and velocity are obtained in each fitting window. The resultant M_2 and S_2 phase velocities are shown in Figures 4a and 4b, respectively. I have repeated the calculation using fitting windows ranging 300-600 km one side and found that their means do not change much (but that uncertainties are large for smaller fitting windows). The spring-neap cycle has long wavelength and noisy phase (refer to Figure 2e). Therefore, the group velocity is calculated using a fitting window of 10° by 10° . The propagation velocity is first determined in the south-north direction and then adjusted by $\cos \theta_c$, where θ_c is its propagation direction with respect to north. The resultant group velocity is shown in Figure 4c.

Comparisons of the observed and theoretical velocities reveal a degree of uncertainty in observations (Figures 4a-4c). To characterize the latitudinal dependence, zonal-mean velocities are calculated (Figures 4g-4i). In these panels, the color-coded lines are the zonal-mean theoretical velocities shown in Figures 4d-4f. The black lines denote the zonal-mean observed velocities shown in Figures 4a-4c. For all quantities, the observed and theoretical values agree well—the black lines and the corresponding color-coded lines almost overlap. Point-by-point comparisons of the observed and theoretical velocities are shown by histograms of their differences (Figures 4j-4l). For the M_2 and S_2 phase velocities, the root-mean-square (RMS) differences are 0.07 and 0.08 m/s, respectively. For the spring-neap cycle, the RMS

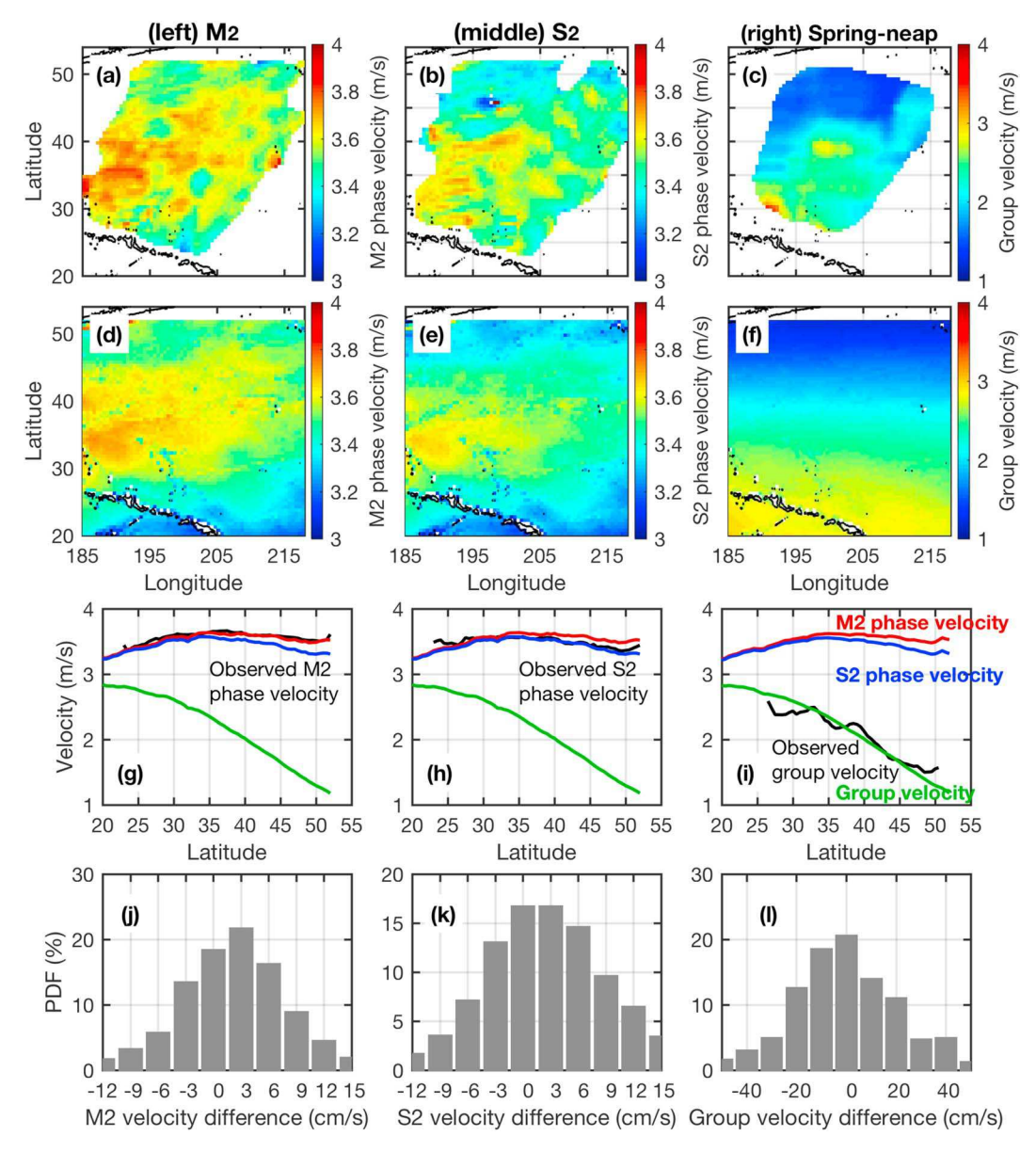


Figure 4. Comparisons of the observed and theoretical velocities. (left) M_2 . (middle) S_2 . (right) The spring-neap cycle. (a-c) Observed velocities determined from phase gradients of the satellite observed internal tides shown in Figures 2c-2e. The fitted results are discarded when there are <75% of valid phase data. (d-f) Theoretical velocities estimated using the WOA13 annual-mean ocean stratification. (g-i) Zonal-mean velocities. The observed values are in black. The theoretical values are labeled by colored lines. (j-k) Histograms of the point-by-point differences between the observed and theoretical velocities.

difference is about 0.23 m/s. The discrepancies can be explained by uncertainties associated with both the theoretical and observational methods. The good agreements between the observed and theoretical velocities confirm that the phase and group velocities estimated from satellite altimetry are reliable.

5. Summary

The superposition of two waves of slightly different wavelengths has long been used to illustrate the distinction of phase velocity and group velocity. In this paper, the first-mode M_2 and S_2 internal tides exemplify such a two-wave model in the natural ocean. The M_2 and S_2 internal tides have a slight difference in frequency ($\approx 3\%$). Their superposition forms a slowly varying spring-neap cycle, with the spring and neap beats corresponding to their in-phase and out-of-phase locations, respectively. The two-wave model is developed by adding the phase information. The results show that the spring-neap cycle propagates like a wave, where its frequency,

wavelength, and phase are the differences of M_2 and S_2 internal tides. In this model, M_2 and S_2 internal tides travel at their respective phase velocity, while the spring-neap cycle travels at the group velocity.

A new method is presented to calculate the group velocity of long-range internal tides from satellite altimetry. The phase velocities of M_2 and S_2 internal tides are determined from their spatial gradients or wave number spectra (Ray & Zaron, 2016; Zhao et al., 2016). Here the group velocity is determined from phase gradients of the spring-neap cycle, which is the phase difference of M_2 and S_2 . In the North Pacific Ocean, the observed phase and group velocities agree very well with the theoretical phase and group velocities estimated using the WOA13 annual-mean ocean stratification. Along a 3,400 km beam, the travel times at phase velocity and group velocity are about 11 and 21 days, respectively.

6. Implications

Phase velocity and group velocity each has its physical meaning and practical applications. Phase velocity is the propagation speed of M_2 or S_2 internal tides in the ocean. Phase is thus an important parameter in internal tide models (Ray & Zaron, 2016; Zhao et al., 2016). Correct phase in internal tide models is important to make internal tide corrections for the next-generation Surface Water Ocean Topography (SWOT) mission (Fu et al., 2012) and field measurements (Zaron & Ray, 2017). Phase velocity is mainly determined by ocean stratification; therefore, the variability of phase velocity can be used to infer the global ocean change by a technique called ITOT (Internal Tide Oceanic Tomography) (Zhao, 2016).

Group velocity is the speed of the wave energy being transported. The global internal tide is generated by the barotropic tide at a rate of about 1 TW (Egbert & Ray, 2000). A significant fraction of the converted energy is transported away by internal tides. To understand where and how the internal tide energy eventually dissipates (Munk & Wunsch, 1998; Wunsch & Ferrari, 2004), it is important to quantify the transport rate by internal tides (e.g., Alford & Zhao, 2007). Group velocity is an indicator of the transport capability of internal tides. It may provide constraints on the pathways of internal tidal energy in the global ocean. It should be useful to build a link of the internal tide energy to field-measured ocean mixing (e.g., Kunze, 2017; Waterhouse et al., 2014; Whalen et al., 2012).

Acknowledgments

This work was supported by the National Science Foundation (OCE1634041) and the National Aeronautics and Space Administration (NNX17AH14G and NNX17AH57G). The author thanks Peter Rhines and Eric D'Asaro for their useful suggestions. This paper was greatly improved with suggestions from two anonymous reviewers. The author appreciates their time and help. The satellite altimeter products were produced by Ssalto/Duacs and distributed by AVISO (Archiving, Validation, and Interpretation of Satellite Oceanographic Data), with support from CNES (http://www.aviso.altimetry.fr). The World Ocean Atlas 2013 is produced and made available by NOAA National Oceanographic Data Center (https://www.nodc.noaa.gov/ OC5/woa13/). All data products presented in this paper are in the supporting information (Data Set S1). Please contact the author for further instructions

(zzhao@apl.washington.edu).

References

Alford, M. H., & Zhao, Z. (2007). Global patterns of low-mode internal-wave propagation. Part II: Group velocity. Journal of Physical Oceanography, 37, 1849-1858.

Chelton, D. B., deSzoeke, R. A., Schlax, M. G., El Naggar, K., & Siwertz, N. (1998). Geographical variability of the first baroclinic Rossby radius of deformation. Journal of Physical Oceanography, 28(3), 433-460.

Egbert, G. D., & Ray, R. D. (2000). Significant dissipation of tidal energy in the deep ocean inferred from satellite altimeter data. Nature, 405, 775-778. https://doi.org/10.1038/35015531

Fu, L.-L., Alsdorf, D., Morrow, R., Rodriguez, E., & Mognard, N. (2012). SWOT: The Surface Water and Ocean Topography Mission—Wide-swath altimetric measurement of water elevation on Earth, JPL publication 12-05. Pasadena, CA: Jet Propulsion Laboratory, California Institute of

Garrett, C., & Kunze, E. (2007). Internal tide generation in the deep ocean. Annual Review of Fluid Mechanics, 39, 57-87. https://doi.org/10.1146/annurev.fluid.39.050905.110227

Gill, A. E. (1982). Atmosphere-ocean dynamics (662 pp.). New York: Academic Press.

Kunze, E. (2017). Internal-wave-driven mixing: Global geography and budgets. Journal of Physical Oceanography, 47, 1325-1345. https://doi.org/10.1175/JPO-D-16-0141.1

Lamb, H. (1916). Hydrodynamics (706 pp.). Cambridge: Cambridge University Press.

Lighthill, J. (1978). Waves in fluids (504 pp.). Cambridge: Cambridge University Press.

Locarnini, R. A., Mishonov, A. V., Antonov, J. I., Boyer, T. P., Garcia, H. E., Baranova, O. K., . . . Seidov, D. (2013). World Ocean Atlas 2013, Temperature (Vol. 1, p. 40). NOAA Atlas NESDIS 73, Silver Spring, MD. Retrieved from http://data.nodc.noaa.gov/woa/WOA13/ DOC/woa13 vol1.pdf

Merrifield, M. A., & Holloway, P. E. (2002). Model estimates of M_2 internal tide energetics at the Hawaiian Ridge. Journal of Geophysical Research, 107(C8), 3179, https://doi.org/10.1029/2001JC000996

Munk, W. (1981). Internal waves and small-scale processes. In B. A. Warren & C. Wunsch (Eds.), Evolution of physical oceanography (pp. 264-291). Cambridge, MA: MIT Press.

Munk, W., & Wunsch, C. (1998). Abyssal recipes II: Energetics of tidal and wind mixing. Deep Sea Research Part I: Oceanographic Research Papers, 45(12), 1977 - 2010. https://doi.org/10.1016/S0967-0637(98)00070-3

Olbers, D. J. (1983). Models of the oceanic internal wave field. Reviews of Geophysics and Space Physics, 21(7), 1567 – 1606. https://doi.org/10.1029/RG021i007p01567

Rainville, L., & Pinkel, R. (2006). Propagation of low-mode internal waves through the ocean. Journal of Physical Oceanography, 36, 1220-1236. https://doi.org/10.1175/JPO2889.1

Ray, R. D., & Cartwright, D. E. (2001). Estimates of internal tide energy fluxes from TOPEX/Poseidon altimetry: Central North Pacific. Geophysical Research Letters, 28(7), 1259-1262, https://doi.org/10.1029/2000GL012447

Ray, R. D., & Mitchum, G. T. (1996). Surface manifestation of internal tides generated near Hawaii. Geophysical Research Letters, 23(16), 2101-2104.



- Ray, R. D., & Zaron, E. (2016). M₂ internal tides and their observed wavenumber spectra from satellite altimetry. *Journal of Physical Oceanography*, 46(1), 3–22. https://doi.org/10.1175/JPO-D-15-0065.1
- Rayleigh, L. (1877). On progressive waves. Proceedings London Mathematical Society, 9, 21-26.
- Reynolds, O. (1877). On the rate of progression of groups of waves and the rate at which energy is transmitted. *Nature*, 16, 343–344. Russell, S. J. (1844). Report on waves. *British Association for the Advancement of Science Report*, 13, 311–390.
- Smith, W. H. F., & Sandwell, D. T. (1997). Global sea floor topography from satellite altimetry and ship depth soundings. *Science*, 277, 1956–1962.
- Stokes, G. G. (1876). Smith's Prize examination paper for February 2, 1876, question 11. In *Mathematical and Physical Papers 5*. Cambridge University Press.
- Waterhouse, A. F., MacKinnon, J. A., Nash, J. D., Alford, M. H., Kunze, E., Simmons, H. L., . . . Lee, C. M. (2014). Global patterns of diapycnal mixing from measurements of the turbulent dissipation rate. *Journal of Physical Oceanography*, 44, 1854–1872. https://doi.org/10.1175/JPO-D-13-0104.1
- Whalen, C. B., Talley, L. D., & MacKinnon, J. A. (2012). Spatial and temporal variability of global ocean mixing inferred from Argo profiles. *Geophysical Research Letters*, 39, L18612. https://doi.org/10.1029/2012GL053196
- Wunsch, C. (1975). Internal tides in the ocean. Reviews of Geophysics and Space Physics, 13, 167–182.
- Wunsch, C., & Ferrari, R. (2004). Vertical mixing, energy, and the general circulation of the oceans. *Annual Reviews Fluid Mechanics*, *36*, 281–314. https://doi.org/10.1146/annurev.fluid.36.050802.122121
- Zaron, E. D., & Ray, R. D. (2017). Using an altimeter-derived internal tide model to remove tides from in situ data. *Geophysical Research Letters*, 44, 4241–4245. https://doi.org/10.1002/2017GL072950
- Zhao, Z. (2016). Internal tide oceanic tomography. *Geophysical Research Letters*, 43, 9157–9164. https://doi.org/10.1002/2016GL070567 Zhao, Z. (2017). The global mode-1 S₂ internal tide. *Journal of Geophysical Research: Oceans*, 122. https://doi.org/10.1002/2017JC013112 Zhao, Z., Alford, M. H., Girton, J. B., Rainville, L., & Simmons, H. L. (2016). Global observations of open-ocean mode-1 M₂ internal tides. *Journal of Physical Oceanography*, 6, 1657–1684. https://doi.org/10.1175/JPO-D-15-0105.1
- Zweng, M., Reagan, J., Antonov, J., Locarnini, R., Mishonov, A., Boyer, T., . . . Biddle, M. (2013). World ocean atlas 2013: Salinity (Vol. 2, p. 39). NOAA Atlas NESDIS 74, Silver Spring, MD. Retrieved from http://data.nodc.noaa.gov/woa/WOA13/DOC/woa13_vol2.pdf